Eric Senéterre, MD • Patrick Taourel, MD • Yves Bouvier, MD • Jean Pradel, MD
Bernard Van Beers, MD • Jean-Pierre Daures, MD • Jacques Pringot, MD
Didier Mathieu, MD • Jean-Michel Bruel, MD

Detection of Hepatic Metastases: Ferumoxides-enhanced MR Imaging versus Unenhanced MR Imaging and CT during Arterial Portography[1]

PURPOSE: **To prospectively compare the diagnostic accuracy of computed tomography (CT) during arterial portography (CTAP) with that of unenhanced and ferumoxides-enhanced magnetic resonance (MR) imaging at 0.5 T in the detection of hepatic metastases.**

MATERIALS AND METHODS: **Four pairs of radiologists independently assessed the metastatic involvement of 134 hepatic segments (31 with and 103 without metastasis) in 17 patients at unenhanced and ferumoxides-enhanced spin-echo and gradient-echo MR imaging (alone and in combination) and at CTAP. The diagnostic performance of the various imaging modalities was assessed by means of receiver operating characteristic analysis.**

RESULTS: **The accuracy of CTAP, unenhanced MR imaging (combined unenhanced sequences), and ferumoxides-enhanced MR imaging (combined contrast material–enhanced sequences) was 0.925, 0.908, and 0.951, respectively. Ferumoxides-enhanced MR imaging was significantly more accurate ($P < .05$) than unenhanced MR imaging and CTAP. When 14 segments containing cysts were excluded, the difference between ferumoxides-enhanced MR imaging and CTAP was no longer statistically significant ($P = .1$).**

CONCLUSION: **Ferumoxides-enhanced MR imaging is more accurate than unenhanced MR imaging and at least as accurate as CTAP for the detection of hepatic metastases.**

PREOPERATIVE detection of liver metastases is a crucial issue in the care of patients with known primary cancer because the number, size, and distribution of lesions determine the therapeutic options (1–4). Computed tomography (CT) during arterial portography (CTAP) is currently considered the most sensitive nonsurgical imaging modality for the detection of liver metastases, with reported sensitivities ranging from 81% to 93% (5–8). Because of its invasive nature, however, this modality is not performed for routine screening. Furthermore, CTAP is associated with a substantial false-positive rate (9–11).

Ferumoxides is a tissue-specific magnetic resonance (MR) imaging contrast agent used for the detection of hepatic tumors. The first results at ferumoxides-enhanced MR imaging were reported under different names (Ferrite or AMI-25; Advanced Magnetics, Cambridge, Mass and Guerbet, Aulnay sous Bois, France). Ferumoxides is now the generic name assigned by the United States Adopted Names Council of the American Medical Association. In a recent editorial, Weissleder (12) reviewed the published data on the clinical use of ferumoxides: Most of these reports showed an increased number of detectable liver lesions. He stressed the need for comparison of ferumoxides-enhanced MR imaging with unenhanced MR imaging and CTAP, with a reliable standard of reference and the use of gradient-echo (GRE) sequences.

The objective of our study was to prospectively compare the accuracy of CTAP with that of unenhanced and ferumoxides-enhanced MR imaging at 0.5 T in the detection of hepatic metastases. We used findings at intraoperative ultrasound (US) as the standard of reference for pathologic proof (13–15) and conducted a receiver operating characteristic (ROC) analysis on a segment-by-segment basis.

MATERIALS AND METHODS

Patients

From July 1993 to February 1994, 23 consecutive patients were referred to Hôpital St Eloi for preoperative assessment of liver metastases. Patients were included in this study if they (*a*) had primary malignancy and suspected liver metastases depicted at contrast material–enhanced CT and (*b*) were a candidate for resection of the hepatic metastases. Six patients were excluded because they did not undergo surgery ($n = 5$) or because intraoperative US was not performed for technical reasons ($n = 1$). Our final study group comprised 17 patients (14 men, three women, aged 40–80 years [mean, 68 years]). Each patient underwent CTAP, unenhanced and ferumoxides-enhanced MR imaging, and subsequent surgical hepatic explora-

Index terms: Computed tomography (CT), comparative studies • Iron • Liver neoplasms, CT, 761.12112 • Liver neoplasms, MR, 761.12143 • Magnetic resonance (MR), comparative studies • Magnetic resonance (MR), contrast enhancement, 761.12143 • Portography, 952.1242

Abbreviations: CTAP = CT during arterial portography, GRE = gradient echo, ROC = receiver operating characteristic, SE = spin echo.

Radiology 1996; 200:785–792

[1] From the Department of Medical Imaging Hôpital St Eloi, 2 Ave Bertin-Sans, 34295 Montpellier 5, France (E.S., P.T., Y.B., J. Pradel, J.M.B.); the Department of Radiology and Medical Imaging, Hôpital St Luc, Brussels, Belgium (B.V.B., J. Pringot); the Department of Medical Information, Hôpital G. Doumergue, Nimes, France (J.P.D.); and the Department of Medical Imaging, Hôpital Henry Mondor, Creteil, France (D.M.). From the 1995 RSNA scientific assembly. Received January 23, 1996; revision requested March 5; revision received April 18; accepted April 29. **Address reprint requests to** E.S.

See also the editorial by Soyer (pp 610–611) in this issue.

tion including intraoperative US within a period of less than 1 month. This study was performed as part of the phase IIIb trial (after file submission) of ferumoxides in Europe. The protocol was submitted to and approved by the ethics committee of Montpellier Hospital. Informed consent was obtained from all patients. The primary tumor originated in the following sites: colon (n = 9), rectum (n = 6), stomach (n = 1), and pancreas (n = 1). The suspected metastases were metachronous in 14 patients and synchronous in three.

Table 1
Individual and Mean A_Z for Each Modality

Imaging Technique	A_Z Index				
	Pair 1	Pair 2	Pair 3	Pair 4	Mean A_Z Index*
CTAP	0.896	0.937	0.940	0.927	0.925 ± 0.020†
Unenhanced MR imaging					
GRE	0.893	0.909	0.868	0.907	0.894 ± 0.019
SE	0.821	0.778	0.845	0.861	0.826 ± 0.036
GRE and SE combined	0.914	0.891	0.902	0.924	0.908 ± 0.014†
Ferumoxides-enhanced MR imaging					
GRE	0.937	0.964	0.946	0.936	0.946 ± 0.013†‡
SE	0.909	0.874	0.934	0.923	0.910 ± 0.026†
GRE and SE combined	0.943	0.959	0.950	0.951	0.951 ± 0.007†‡§‖
Unenhanced and ferumoxides-enhanced MR imaging combined	0.957	0.949	0.945	0.947	0.950 ± 0.005†‡§

* Data are mean ± standard deviation.
† Mean A_Z index was higher ($P < .05$) than that with unenhanced SE sequence (2,000/40, 80, 120).
‡ Mean A_Z index was higher ($P < .05$) than that with unenhanced GRE sequence (170/12, with 70° flip angle).
§ Mean A_Z index was higher ($P < .05$) than that with combined MR sequences.
‖ Mean A_Z index was higher ($P < .05$) than that with CTAP.

CTAP

Limited visceral angiography with 10–20 mL of iodinated contrast material was performed in all patients to position the tip of a 5-F end-hole catheter (Cordis, Roden, The Netherlands) in the proximal superior mesenteric artery to determine the infusion capacity of the vessel and to exclude an aberrant right hepatic artery. The patients were subsequently transferred to the CT scanner for CTAP, where they received 200 mL of iodinated contrast material (sodium and meglumine ioxaglate, 200 mg of iodine per milliliter [Hexabrix 200; Guerbet, Aulnay sous Bois, France]) at a rate of 2 mL/sec through a power injector (Medrad, Pittsburgh, Pa). Incremental CT examination of the liver was performed (Somatom DRH; Siemens, Erlangen, Germany); 8-mm-thick sections were obtained at a rate of 7.5 images per minute, with an intersection gap of 2 mm. The mean number of CTAP sections throughout the liver was 15, corresponding to a mean acquisition time of 1 minute 55 seconds. The first section was obtained in the upper part of the liver, 20 seconds after initiation of infusion to obtain images during the portal phase of arterial infusion.

MR Imaging

MR imaging was performed with a 0.5-T superconductive imaging system (MR Max; GE Medical Systems, Milwaukee, Wis). Ferumoxides (Endorem; Guerbet) was administered at a dose of 15 μmol of iron per kilogram of body weight. The ferumoxides suspension was diluted in 100 mL of 5% dextrose solution and was administered intravenously in 30 minutes. Before and 1 hour after initiation of the injection, long-repetition-time, spin-echo (SE) (repetition time [msec]/echo time [msec] = 2,000/40, 80, 120) imaging was performed in the entire liver in the transverse plane. Imaging was performed with the following parameters: 12 sections, 10-mm-thick sections, 5-mm intersection gap, 256 × 192 matrix, 420 × 420-mm field of view, two signals acquired, and use of superior and inferior presaturation bands. Gradient moment nulling and respiratory reordering were not used because the first increases the signal of flowing blood and reduces the number of sections and the second was not efficient with our MR unit.

Before and 1 hour after injection of ferumoxides, breath-hold GRE imaging was performed with the following parameters: five sections, 10-mm-thick sections, 2-mm intersection gap, 256 × 192 matrix, 420 × 315-mm rectangular field of view, one signal acquired, and acquisition time of 31 seconds. Before each series of five sections, patients were asked to maintain a maximal deep breath hold for the time of imaging. Acquisition of three to four series was necessary to explore the entire liver in the transverse plane.

Instead of comparing images obtained with the same sequence before and after administration of contrast material, we chose to compare images obtained with optimized sequences for the two situations. A repetition time of 170 msec was chosen in both cases to allow five sections to be acquired in one breath hold. The echo time was set to the minimum value (12 msec) on our MR unit. After ferumoxides administration this echo time allowed sufficient T2* weighting, and very low signal intensity was present in liver parenchyma (close to that of background noise) on MR images.

Before contrast material administration, the flip angle was 70° for intense T1 weighting. Findings in previous studies have shown that T1 weighting should be avoided in ferumoxides-enhanced SE sequences because it reduces the contrast-to-noise ratio and the detection rate of liver metastases (15–20). The flip angle in our contrast-enhanced GRE sequence was therefore lowered to 45° to obtain the lowest T1 weighting with an acceptable signal-to-noise ratio. This sequence remains moderately T1 weighted, but further reduction of the angle markedly decreased the signal-to-noise ratio on the images acquired with our MR unit and was considered to be unacceptable.

Intraoperative US

Intraoperative US was performed by an experienced radiologist (E.S.), with a high-resolution 7.5-MHz intraoperative US probe (scanner model 1849, B & K Medical France, Mennecy, France; Sonolayer SAL35A, Toshiba, Nasu, Japan, respectively). The sterilized probe was applied on all palpable parts of the liver after mobilization and bimanual palpation of the liver by the surgeon. The operator checked the lesions suspected at preoperative imaging, carefully looking for additional metastases and for other types of lesions such as cyst, hemangioma, or focal steatosis. In addition, the operator noted the segmental location of all metastatic and benign nodules. The results of this examination served as a segment-by-segment standard of reference for the study.

Forty-one metastases ranging from 2 to 85 mm in diameter (mean, 22 mm ± 17 [standard deviation]) were detected at intraoperative US. Fifteen of these metastases were less than 10 mm in diameter. If the larger lesions in each segment are considered, which is relevant in a segment-by-segment analysis of metastatic involvement, 31 metastases were detected that ranged from 2 to 85 mm in diameter (mean, 27 mm ± 16). Five of these metastases were less than 10 mm in diameter.

Pathologic Examination

Eleven of the 17 patients underwent surgical resection; four had a catheter placed into the hepatic artery for chemotherapy; and two had peritoneal carcinomatosis, which precluded hepatic resection or catheter implantation. The resected specimens represented 31 complete segments and four cuneiform resections for metastases. The pathologist was aware of the results at intraoperative US. The results confirmed the metastases suspected at intraoperative US in all resected specimens (20 metastases), which indicated the absence of false-positive results at intraoperative US in this subgroup of segments. Four of the 11 patients underwent surgery at another institution (nine complete segments); no systematic slicing of the speci-

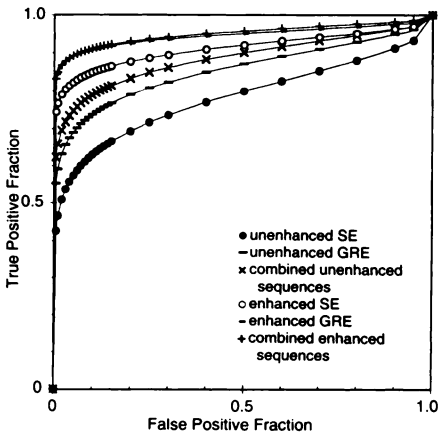

Figure 1. ROC curves indicate the relative accuracy with which metastases are detected with unenhanced and ferumoxides-enhanced MR imaging. (The ROC curve for the unenhanced and contrast-enhanced sequences combined is similar to that for the contrast-enhanced sequences combined.)

mens was done. Therefore, false-negative intraoperative US findings cannot be excluded in these cases. Specimens from seven of the 11 patients (22 complete segments) were sliced into 1-cm-thick sections. Two additional metastases less than 1 cm in diameter were found in segments already involved with larger lesions. These results did not modify the intraoperative US segment-by-segment standard of reference. The standard of reference in this study was therefore pathologic analysis in 22 segments and intraoperative US in the remaining 112 segments.

Image Review

Two sets of images obtained with each of the five modalities (CTAP, unenhanced and ferumoxides-enhanced SE and GRE MR imaging) were placed in individual folders after the patient's name was masked. Our study was conducted on a segment-by-segment basis. As our objective was to assess the ability of readers to detect lesions and not to localize them, we tried to prevent mislocation of the lesions by the readers. Hepatic segmentation according to the Couinaud numbering system (21,22) was drawn directly by one radiologist (E.S.) not involved in reading sessions on one set of images (23). This set served as a guide to avoid disagreement about the segmental location of the lesions.

The examinations were reviewed by four independent pairs of two experienced radiologists (J. Pradel and J.M.B., D.M. and Alain Duron, P.T. and Y.B., or B.V.B. and J. Pringot), who knew that the patients were referred for preoperative assessment of liver metastases but did not know any other information about the patients' history. For each patient, the four pairs of readers reviewed images obtained with the five individual modalities and three combined modalities (unenhanced sequences combined, ferumoxides-enhanced sequences combined, and unenhanced and ferumoxides-enhanced sequences combined). This represented a total of 544 readings for all patients (136 readings per pair of readers).

For each pair of reviewers, the reviewing procedure was performed in five sessions at 2-week intervals. At each session, images obtained with one individual modality per patient were reviewed. To limit learning bias, we introduced a balanced permutation of the order of the patient images in the reading sessions and of the order of the individual modality images for each patient in the five reading sessions. These orders were different for each pair of readers (24). Images obtained with each combined modality were evaluated immediately after each pair of readers had reviewed the images obtained with the last individual modality composing this combined modality. Eight modalities per patient were reviewed, therefore, in five reading sessions.

In the 17 patients, a total of 136 segments were represented. Two segments were excluded, one because of the uncertain nature of a lesion that could not be sampled at biopsy or removed. In the other case, two segments were totally occupied with a single metastasis and were considered to be a single segment. A total of 134 segments (31 with at least one metastasis and 103 without metastasis) were entered into the ROC analysis. The number of metastatic segments per patient ranged from 0 to 5 (mean, 1.8). Five metastatic segments contained only metastasis(es) less than 1 cm in diameter. Fourteen segments contained at least one benign liver cyst, and two of the 14 segments contained both metastasis and cyst. In seven of these segments, the larger cyst was less than 5 mm in diameter. No hemangiomas or focal steatosis were observed in our series.

Each of the two readers were asked to state in consensus for each segment whether they were able to ascertain the presence or absence of metastases. They assigned one of five confidence levels (5 = metastasis definitely present, 4 = metastasis probably present, 3 = undetermined, 2 = probably no metastasis present, 1 = definitely no metastasis present). When a lesion invaded two or more segments, readers were asked to consider the lesion in only the segment mainly involved and to assess the probability of another lesion in the other segment(s).

Statistical Analysis

For each imaging modality, a binomial ROC curve was fitted to each pair's confidence rating data by using a maximum likelihood estimation (25). The diagnostic accuracy of each imaging modality for each pair of readers was estimated by calculating the area under the ROC curve (A_z index) (26). The differences between imaging modalities in terms of the mean areas under the ROC curves (mean A_z index) were statistically analyzed by using the two-tailed Student *t* test for paired data (27). The 95% confidence intervals representing the range (lower boundary, upper boundary) within which the true value of the difference between two accuracies plausibly lies, were calculated for the main comparisons when the difference was not statistically significant ($P > .05$) (28). Composite ROC curves representing the performance of all pairs of readers as a single pair were obtained for each imaging modality by using the maximum-likelihood curve-fitting algorithm to rate the pooled data of the four pairs of readers (27).

Differences between ROC curves of individual pairs of readers were not tested because we used multiple segments from each patient. The algorithms used for statistical comparison of ROC curves were estimated from correlated data sets and account for case sample variation. Therefore, any correlation between reading of different segments served to reduce the effective size of the segment sample, thereby potentially causing statistical significance to be overestimated with the algorithms (27,29). The Student *t* test for paired data does not attempt to account for case sample variation, and the statistical significance of the difference between mean A_z values was not affected by our use of multiple segments from each patient (27,29).

Given the abnormally high rate of segments containing cysts in our population, we performed a second ROC analysis in a subpopulation of segments without cysts (120 segments [29 with at least one metastasis and 91 without metastasis]) for CTAP and ferumoxides-enhanced MR imaging.

To compare the risk of false-positive results in the presence of cysts at CTAP and ferumoxides-enhanced imaging, we used the confidence level ratings for each pair of readers in a subgroup of nonmetastatic segments containing cysts. Ratings of 3, 4, and 5 were considered false-positive results. Comparison between values for CTAP and ferumoxides-enhanced imaging were obtained by means of paired Student *t* tests.

RESULTS

The A_z values for each of the four pairs of readers with all modalities are shown in Table 1. ROC curves constructed on the basis of pooled data from all pairs of readers are shown in Figures 1 and 2a.

Ferumoxides-enhanced MR Imaging

For ferumoxides-enhanced MR imaging, the combination of GRE and SE sequences provided the greatest accuracy, with a mean A_z of 0.951. No statistically significant difference was found between the three ferumoxides-enhanced imaging sequences (GRE, SE, and GRE and SE combined) (Table 2). False-negative and false-positive results were compared for each seg-

ment and for each group of readers in the noncystic group of segments (116 scores concerning metastatic segments and 364 scores concerning nonmetastatic segments). We observed 10 false-negative results (ratings of 1, 2, or 3) and 42 false-positive results (ratings of 3, 4, or 5) for the SE sequence when a true result was obtained with the GRE sequence, and we observed two false-negative and eight false-positive results for the GRE sequence when a true result was obtained with the SE sequence.

Unenhanced versus Ferumoxides-enhanced MR Imaging

For unenhanced MR imaging, the combined unenhanced sequences provided the highest accuracy, with a mean A_z of 0.908. Accuracy with the ferumoxides-enhanced SE and GRE sequences was statistically superior to that with the corresponding unenhanced sequences ($P = .002$ for SE imaging, $P = .016$ for GRE imaging). Accuracy with the combined contrast-enhanced sequences was significantly greater ($P = .02$) than with the combined unenhanced sequences (Fig 3). No metastatic segment was missed with the combined contrast-enhanced sequences that was correctly scored with the combined unenhanced sequences. Accuracy with the combination of unenhanced and contrast-enhanced sequences was not statistically different ($P = .83$) from accuracy with the combination of contrast-enhanced sequences.

CTAP versus Ferumoxides-enhanced MR Imaging

Accuracy with the combined contrast-enhanced MR sequences was significantly greater ($P = .048$) than with CTAP (Fig 4). No statistically significant difference was observed in accuracy with CTAP versus that with contrast-enhanced GRE imaging ($P = .09$), contrast-enhanced SE imaging ($P = .42$), and unenhanced and contrast-enhanced MR imaging combined ($P = .15$).

Because of the large number of segments containing cysts (10%), we performed another ROC analysis after excluding these segments, for a subpopulation of 120 segments (29 with and 91 without metastasis). Results are shown in Table 3 for CTAP and ferumoxides-enhanced imaging. No statistically significant difference was found between the accuracies of CTAP and contrast-enhanced MR imaging (contrast-enhanced SE imaging, $P = .25$; contrast-enhanced GRE imaging, $P = .24$; contrast-enhanced sequences combined, $P = .1$; unenhanced and contrast-enhanced sequences combined, $P = .29$). ROC curves constructed on the basis of pooled data from all pairs of readers for CTAP and the combined contrast-enhanced sequences are shown in Figure 2b. P values and confidence intervals for the comparison of these two modalities are shown in Table 2.

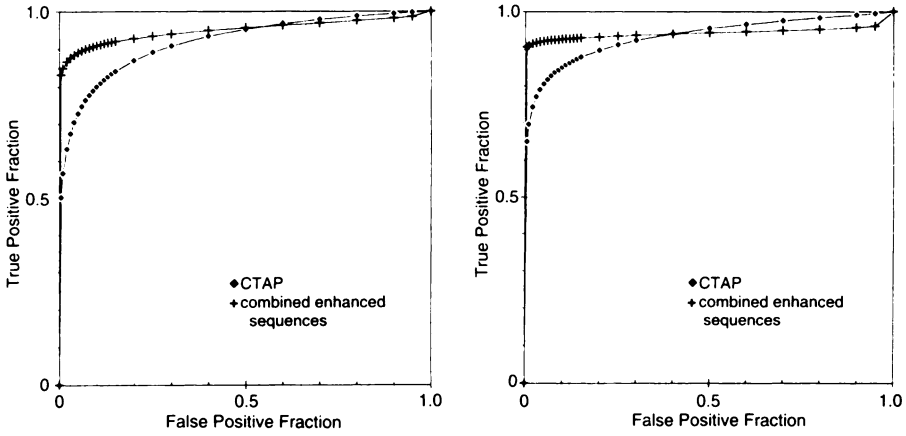

Figure 2. ROC curves for CTAP and combined ferumoxides-enhanced sequences **(a)** for all segments and **(b)** after excluding segments containing cysts.

Table 2
P Values and 95% Confidence Intervals in Nonsignificant Statistical Results

Comparison	Difference in A_z*	P Value	95% Confidence Interval
Enhanced GRE vs enhanced SE	0.036 ± 0.018	.15	−0.023, 0.095
Enhanced GRE-SE vs enhanced SE	0.041 ± 0.015	.08	−0.008, 0.089
Enhanced GRE-SE vs enhanced GRE	0.005 ± 0.004	.31	−0.008, 0.018
Enhanced GRE-SE vs enhanced GRE-SE and unenhanced SE-GRE	0.001 ± 0.005	.84	−0.016, 0.018
Enhanced GRE-SE vs CTAP†	0.019 ± 0.008	.10	−0.007, 0.046

* Data are mean ± standard deviation of the first imaging technique minus the second.
† In segments not containing cyst.

Cysts

In the subgroup of 12 nonmetastatic segments containing cysts, the contrast-enhanced GRE sequence and the combination of unenhanced and contrast-enhanced sequences provided significantly fewer false-positive results than contrast-enhanced SE sequences ($P = .022$ and .014, respectively) and CTAP ($P = .035$ and .037, respectively) (Table 4). The contrast-enhanced GRE sequence alone provided significantly ($P = .006$) fewer false-positive results than the combined contrast-enhanced MR sequences.

DISCUSSION

In previous studies (15–20,29–32), superior detection of hepatic tumors was reported for ferumoxides-enhanced compared with unenhanced MR imaging, except in two studies (31,32). Most of these studies, however, had several limitations: (*a*) an appropriate standard of reference was not used against which tumor detection could be measured (16–20,29–32), (*b*) different histologic types of hepatic tumors were included (18–20,31), and (*c*) GRE sequences were not tested (15,17–20,31–32). Moreover, the specificity cannot be evaluated when comparing the number of detected lesions because of the lack of information concerning true-negative results. Because a lower sensitivity of one modality compared with another can be compensated with a higher specificity, the relative performance of two techniques cannot be accurately determined (25).

In our study, we performed ROC analysis, which is a more precise tool for measuring the diagnostic performance of different imaging procedures since it can take into account the variations in decision criteria (25). Several

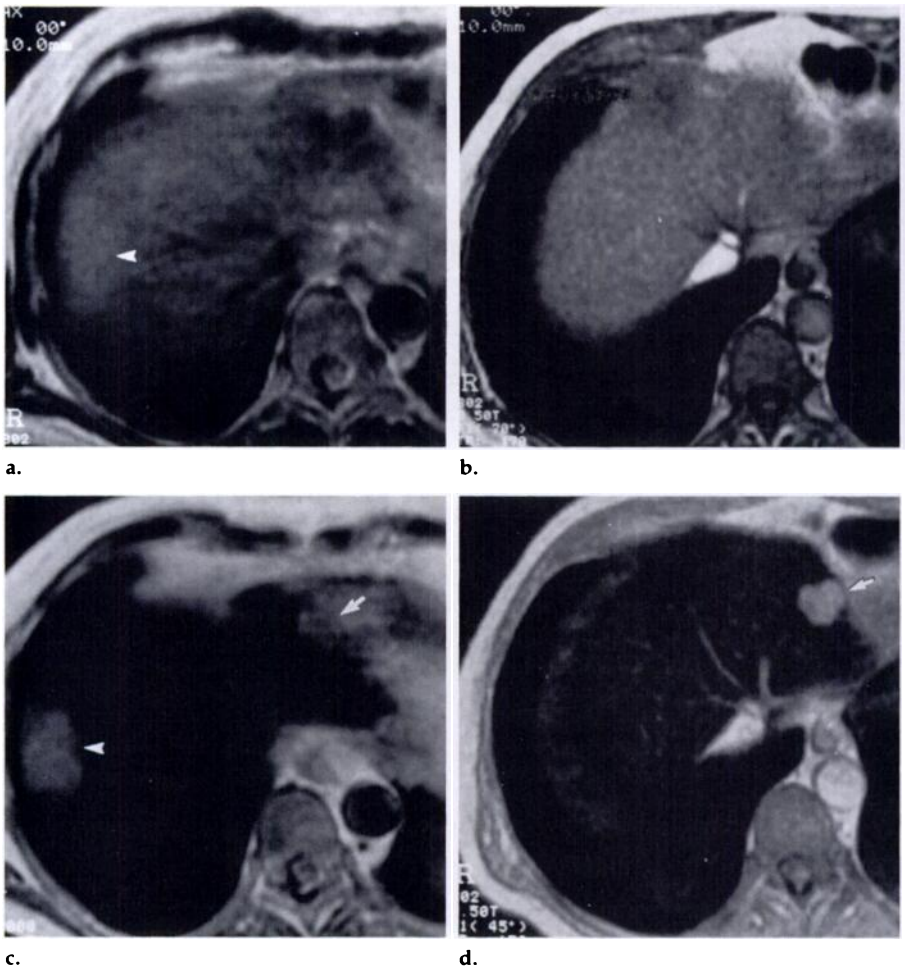

Figure 3. MR images of hepatic metastases from colon cancer. Unenhanced **(a)** SE (2,000/80) and **(b)** GRE (170/12, 70° flip angle) MR images show no lesion in the left lobe of the liver. **(c)** In ferumoxides-enhanced SE (2,000/40) MR image, the metastasis in the left lobe is barely visible (arrow). **(d)** Ferumoxides-enhanced GRE (170/12, 45° flip angle) image clearly shows a 2-cm-diameter metastasis (arrow) in the left lobe. The difficulty in anatomically matching sections is illustrated here. At the level of the left lobe metastasis, a large right lobe metastasis is visible on the unenhanced SE image (arrowhead in **a**) and better seen on the ferumoxides-enhanced SE image (arrowhead in **c**), whereas it was present one section lower on the GRE image (in **d**).

studies comparing techniques for liver imaging by means of ROC curve analysis have been conducted by selecting matching anatomic sections (29,33,34). We chose a segment-by-segment analysis because the matching of anatomic sections is difficult to obtain with imaging techniques performed at different respiratory status. Tilting or deformation of the liver between breath holds of different status and cephalocaudal motion of the liver during SE imaging makes the exact matching of sections practically impossible (Fig 3). With the segment-by-segment method, an overall analysis of each segment is done; therefore, differences in respiratory status, section thickness, and intersection gap are less crucial than they are when sections are matched.

Contrast-enhanced breath-hold GRE imaging was the best individual modality, and the combination of contrast-enhanced SE and GRE imaging was the best modality in general. Findings in previous studies in animals (35) or humans (16,36) have indicated the interest in non-breath-hold GRE imaging after ferumoxides administration. Breath-hold imaging has great diagnostic potential because intravoxel blurring and respiratory motion–induced ghosting artifacts are reduced (37). No statistically significant difference was found among the three ferumoxides-enhanced sequences. Failure to demonstrate a statistically significant difference, however, does not indicate that no difference exists. Because the difference between imaging with the SE sequence and with the combination of SE and GRE sequences was close to statistical significance ($P < .1$) and the confidence interval was large with a lower boundary close to zero, we think that a GRE sequence should be associated with an SE sequence in ferumoxides-enhanced MR imaging.

Our results confirm the superiority of ferumoxides-enhanced MR imaging over unenhanced MR imaging in the detection of liver metastases. Results at imaging with the SE and GRE sequences (alone and in combination) were significantly better after ferumoxides administration. In a previous study with ROC analysis comparing the detection of liver metastases with unenhanced and ferumoxides-enhanced MR imaging at 0.6 T, results with a contrast-enhanced SE sequence (1,500/40) were similar to results obtained with our contrast-enhanced SE sequence (29).

Biliary cysts are the most frequent cause of benign nodules in the liver, and differentiation of cysts from metastases might be troublesome. Among our contrast-enhanced MR imaging techniques, the GRE sequence had the lowest false-positive rate in the group of 12 nonmetastatic segments containing cysts. Because of T1 weighting, cysts had very low signal intensity, close to that of parenchyma, and were probably not seen in most cases. This sequence provided significantly fewer false-positive results than did the contrast-enhanced SE sequence.

It is theoretically possible to differentiate cysts and metastases with late echoes in the contrast-enhanced SE sequence, but this feature was not readily usable in the case of small cysts (Fig 5). Readers obtained a significantly higher false-positive rate for images obtained with the combined enhanced sequences than with the GRE sequence alone. Because the low signal intensity of cysts on contrast-enhanced T2*- and T1-weighted GRE images has not been previously described, to our knowledge, we believe the readers relied more on images obtained with one sequence that depicted nodules (SE) than on images obtained with a sequence that did not depict them (GRE). A thorough knowledge of this feature would probably have increased the specificity of the combined modality.

For detection of hepatic metastases, findings with the combination of all unenhanced and contrast-enhanced sequences were not superior to findings with the combination of all contrast-enhanced sequences. The small confidence interval indicated that a true difference, if any, was small. The interest in unenhanced MR images for ferumoxides-enhanced image analysis may be seen in terms of detection (metastases visualized on unenhanced images and obscured after

ferumoxides administration) or characterization (differentiation of metastases from frequently encountered benign lesions such as cyst and hemangioma). In our study, no metastatic segment was missed with the combined enhanced sequences that was correctly scored with the combined unenhanced sequences. Conversely, cysts were responsible for fewer false-positive results with the GRE sequence than with the combined unenhanced and contrast-enhanced sequences. Therefore, we suspect that unenhanced imaging might be unnecessary in the future in ferumoxides-enhanced MR examinations. To date, ferumoxides-enhanced MR imaging has been studied in clinical trials that include unenhanced and contrast-enhanced imaging, but this protocol will be difficult to implement in clinical practice because of time constraints. Further studies must be conducted to confirm our results and to define characterization criteria for hemangiomas with ferumoxides-enhanced sequences.

Until the advent of superparamagnetic contrast agents, the role of MR imaging in the detection of liver metastases was secondary to CTAP (5,6,8). To our knowledge, ours is the first study to compare ferumoxides-enhanced MR imaging and CTAP. For the comparison of CTAP and combined contrast-enhanced MR imaging in the group of segments without cysts, the *P* value was .1 and the 95% confidence interval was large, with a lower boundary close to zero (−0.007). This means that one can be 97.5% certain that either the accuracy with the combined enhanced sequences is superior to CTAP or the difference is less than 0.007. Therefore, MR imaging with the combination of GRE and SE sequences after ferumoxides administration was at least as accurate as CTAP in the detection of liver metastases.

When segments containing cysts were included, MR imaging with the combination of ferumoxides-enhanced sequences was more accurate than CTAP. The presence of cysts resulted in false-positive results with CTAP in most of the 14 segments containing cysts. The low specificity of CTAP in the presence of both metastases and cysts is well known, and correlation with findings at conventional CT performed before CTAP or at delayed CT performed after CTAP is generally done in clinical practice (9,10). We doubt the efficacy of the additional imaging when cysts are very small, but we decided to rely on the results obtained after exclusion of segments containing cysts in the comparison of CTAP and ferumoxides-enhanced MR imaging because additional CT scans (obtained before or after CTAP) were not available for reading sessions.

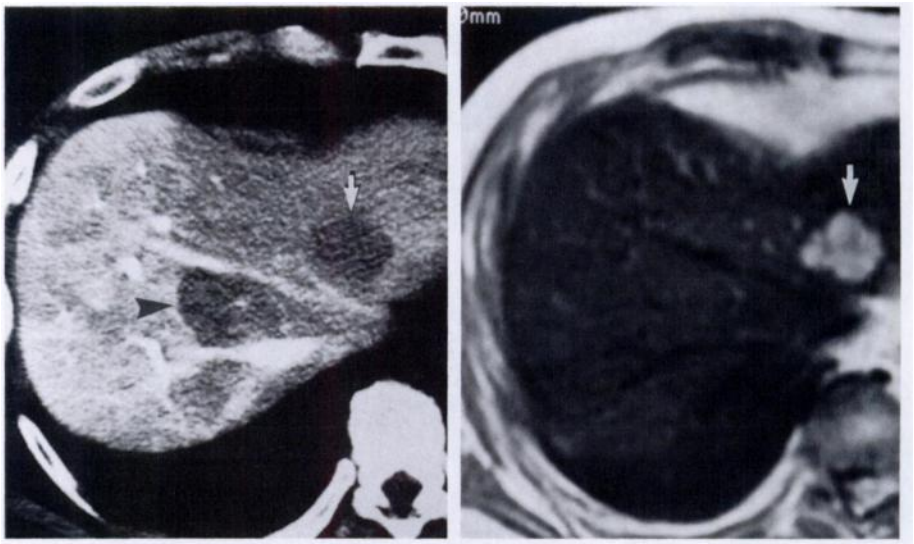

a. b.

Figure 4. False-positive CTAP finding in a patient with hepatic metastasis from colon cancer. **(a)** CTAP scan shows a 3-cm-diameter metastasis in the left lobe (arrow) and a 4-cm-diameter nontumorous vascular defect in the right lobe (arrowhead). **(b)** Ferumoxides-enhanced SE (2,000/40) MR image confirms the presence of the metastasis (arrow), whereas no lesion corresponding to the right-lobe nodule seen on **a** is depicted. No lesion was found in this area at intraoperative US (not shown).

Table 3
Individual and Mean A_Z for CTAP and Ferumoxides-enhanced MR Imaging after Exclusion of Segments with Cysts

Imaging Technique	A_Z Index				
	Pair 1	Pair 2	Pair 3	Pair 4	Mean A_Z Index*
CTAP	0.912	0.944	0.950	0.948	0.938 ± 0.017
Ferumoxides-enhanced MR imaging					
GRE	0.939	0.966	0.950	0.942	0.949 ± 0.012
SE	0.916	0.881	0.943	0.929	0.917 ± 0.027
GRE and SE combined	0.956	0.960	0.958	0.956	0.957 ± 0.002
Unenhanced and ferumoxides-enhanced MR imaging combined	0.956	0.953	0.948	0.949	0.952 ± 0.004

* Data are mean ± standard deviation.

Our study has a number of limitations. First, the available imaging devices were not state-of-the-art equipment. Spiral technology should improve lesion detection with CTAP by enabling use of thinner collimation and overlapping reconstruction, reducing motion artifacts, and suppressing systemic recirculation of the iodinated contrast agent during scanning (9). Our imaging time was long enough to allow systemic recirculation, which may diminish contrast differences between tumors and nonneoplastic hepatic parenchyma. If we consider the metastatic segments that were scored 1, 2, or 3 by at least one pair of readers, however, none of the segments corresponded to inferior segments of the liver (V or VI) that were imaged

Table 4
False-Positive Results for the 12 Nonmetastatic Segments Containing Cysts

Imaging Technique	Reader Pair			
	1	2	3	4
CTAP	9	10	9	4
Ferumoxides-enhanced MR imaging				
GRE	1	6	1	2
SE	5	7	4	5
GRE and SE combined	3	7	3	4
Unenhanced and ferumoxides-enhanced MR imaging combined	3	6	3	3

Note.—Data are number of false-positive results.

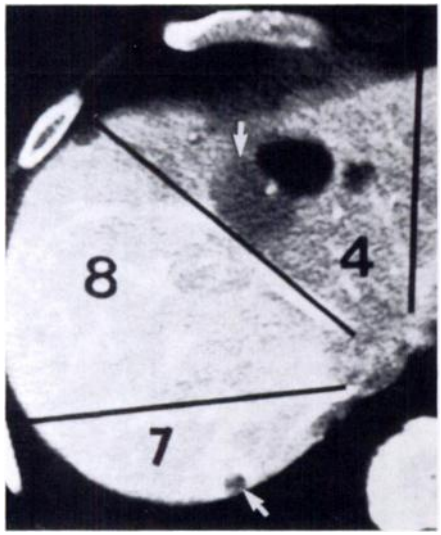

a.

Figure 5. Two hepatic metastases and numerous cysts in a patient with colon cancer. Metastases and cysts were confirmed at intraoperative US and pathologic analysis of two resected segments (IV and VII). **(a)** CTAP scan shows numerous vascular defects, only two of which are related to metastases (arrows). Other vascular defects are cysts. The hepatic segmentation was drawn on the images obtained with each individual modality. This guide to location, represented here for CTAP, was available along with the regular images in the reading sessions to avoid errors in location of the lesions. Numbers are segment numbers. Ferumoxides-enhanced **(b)** GRE (170//12, 45° flip angle), **(c)** SE (2,000/40), and **(d)** SE (2,000/120) MR images were obtained at the level of the large metastasis (arrow) and depict a 3-cm-diameter cyst (arrowhead). The cyst is not seen on **b**, whereas on **c**, metastasis and cyst cannot be differentiated. On **d**, the cyst has a higher signal intensity than the metastasis. Ferumoxides-enhanced **(e)** GRE (170/12, 45° flip angle), **(f)** SE (2,000/40), and **(g)** SE (2,000/120) MR images were obtained at the level of the small metastasis (arrow) and depict a 1-cm-diameter cyst (arrowhead on **f** and **g**). Because of partial volume effect and low signal-to-noise ratio, the differentiation of cyst from metastasis is not straightforward on **f** and **g**, whereas only the metastasis is visible on **e**.

b.

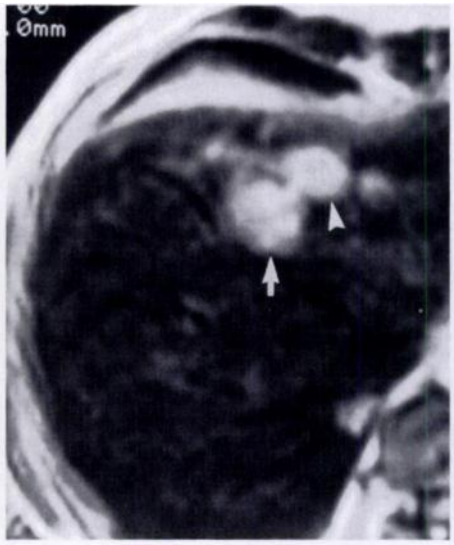

c.

d.

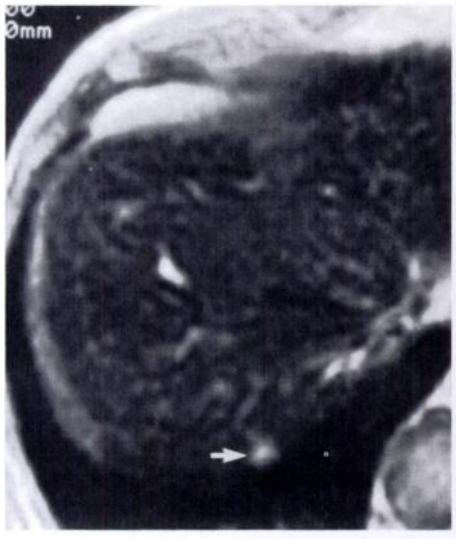

e.

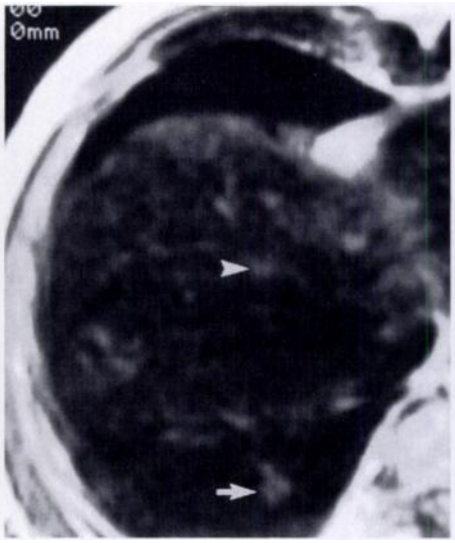

f.

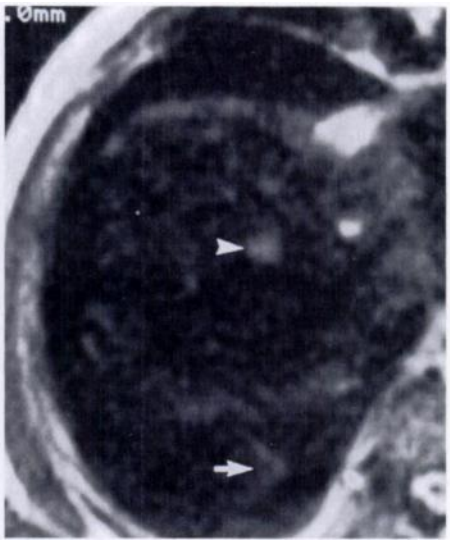

g.

late after the start of contrast material injection.

At MR imaging, respiratory reordering could not be used in SE sequences and we could not avoid some T1 weighting in our breath-hold T2*-weighted GRE sequence. With more recent technologies, we expect an acceptable signal-to-noise ratio with use of a lower flip angle and a potentially better contrast-to-noise ratio and detection rate. Furthermore, the multi-

planar capacity in breath-hold GRE sequences was not used. In a recent article (38), lesion detection with T1-weighted unenhanced GRE sequences in three planes was superior to that in the axial plane alone, especially for lesions smaller than 1 cm in diameter.

Second, because we used segment-by-segment analysis, the number of segments containing only lesions smaller than 1 cm in diameter was low because, in many cases, small lesions were situated in a segment or segments that also contained a larger lesion. The capacity of CTAP and ferumoxides-enhanced MR imaging could not be compared for these particular lesions. In a recent article, Hagspiel et al (15) reported a low sensitivity (56%) in lesion detection for ferumoxides-enhanced MR imaging, which they explained as a result of the high rate of metastases smaller than 1 cm in diameter (41%). Because the main value of CTAP is in the detection of small lesions (9), we cannot exclude that results with CTAP would be better in such cases.

Third, our standard of reference was findings at intraoperative US and pathologic analysis in 22 segments and at intraoperative US alone in 112 segments. In recent studies, the sensitivity of intraoperative US in the detection of hepatic metastases ranged from 80% to 96% (14,15). We therefore cannot exclude false-negative results in our standard of reference. This limitation should not influence the results of a comparative study of imaging modalities, but absolute values of accuracy should be regarded with caution.

In conclusion, ferumoxides-enhanced MR imaging at 0.5 T is at least as accurate as CTAP and more accurate than unenhanced MR imaging in the preoperative assessment of liver metastases. Further studies must be conducted to compare the accuracy of these two techniques with that of spiral CT technology and state-of-the-art MR pulse sequences and for lesions smaller than 1 cm in diameter. Nevertheless, we believe that ferumoxides-enhanced MR imaging is a good alternative to CTAP, which is invasive and expensive. Because ferumoxides-enhanced MR imaging is noninvasive, it may also be used for routine screening. Ferumoxides-enhanced GRE imaging is accurate and should be included in the ferumoxides-enhanced MR protocol. With improvement in sequences and use of the multiplanar capacity of breath-hold sequences, the accuracy of the technique is likely to improve. When this sequence is T1 weighted, it allows good differentiation of metastases from cysts on contrast-enhanced images. For cost effectiveness, unenhanced imaging should be avoided and, therefore, further improvements in sequence design are necessary to help differentiate metastases from other nonmalignant nodules such as hemangiomas on contrast-enhanced images. ■

References

1. Hughes KS, Simon RM, Songhrabodi S, et al. Resection of the liver for colorectal carcinoma metastases: a multi-institutional study of indications for resection. Surgery 1987; 103:278–288.
2. Nordlinger B, Jaeck D, Guiguet M, et al. Surgical resection of hepatic metastases: multicentric retrospective study by the French Association of Surgery. In: Nordlinger B, Jaeck D, eds. Treatment of hepatic metastases of colorectal cancer. Paris, France: Springer, 1992; 129–146.
3. Scheele J, Stang R, Altendorf-Hofmann A, Paul M. Resection of colorectal liver metastases. World J Surg 1995; 19:59–71.
4. Sugarbaker PH. Surgical decision-making for large bowel cancer metastatic to the liver. Radiology 1990; 174:621–626.
5. Nelson RC, Chezmar JL, Sugarbaker PH, Bernardino ME. Hepatic tumors: comparison of CT during arterial portography, delayed CT, and MR imaging for preoperative evaluation. Radiology 1989; 172:27–34.
6. Heiken JP, Weyman PJ, Lee LKT, et al. Detection of focal hepatic masses: prospective evaluation with CT, delayed CT, CT during arterial portography, and MR imaging. Radiology 1989; 171:47–51.
7. Soyer P, Levesque M, Elias D, Zeitoun G, Roche A. Detection of liver metastases from colorectal cancer: comparison of intraoperative ultrasound and CTAP. Radiology 1992; 183: 531–544.
8. Soyer P, Levesque M, Caudron C, Elias D, Zeitoun G, Roche A. MRI of liver metastases from colorectal cancer vs CT during arterial portography. J Comput Assist Tomogr 1993; 17:67–74.
9. Soyer P, Bluemke DA, Fishman EK. CT during arterial portography for the preoperative evaluation of hepatic tumors: how, when and why. AJR 1994; 163:1325–1331.
10. Peterson MS, Baron RL, Dodd GD III, et al. Hepatic parenchymal perfusion defects detected with CTAP: imaging-pathologic correlation. Radiology 1992; 185:149–155.
11. Soyer P, Bluemke DA, Hruban RH, Sitzmann JV, Fishman EK. Hepatic metastases from colorectal cancer: detection and false-positive findings with helical CT during arterial portography. Radiology 1994; 193:71–74.
12. Weissleder R. Liver MR imaging with iron oxides: toward consensus and clinical practice. Radiology 1994; 193:593–595.
13. Charnley RM, Morris DL, Dennison AR, Amar SS, Hardcastle JD. Detection of colorectal liver metastases using intraoperative ultrasonography. Br J Surg 1991; 78:45–48.
14. Soyer P, Elias D, Zeitoun G, Roche A, Levesque M. Surgical treatment of hepatic metastases: impact of intraoperative ultrasound. AJR 1993; 160:511–514.
15. Hagspiel KD, Neidl KF, Eichenberger AC, Weder W, Marincek B. Detection of liver metastases: comparison of superparamagnetic iron oxide–enhanced and unenhanced MR imaging at 1.5 T with dynamic CT, intraoperative US, and percutaneous US. Radiology 1995; 196:471–478.
16. Bellin MF, Souhil Z, Auberton E, et al. Liver metastases: safety and efficacy of detection with superparamagnetic iron oxide in MR imaging. Radiology 1994; 193:657–663.
17. Bruel JM. Superparamagnetic iron oxide for the detection of hepatic lesion with MR imaging: results of a phase III trial (abstr). Radiology 1993; 189(P):273.
18. Stark DD, Weissleder R, Elizondo G, et al. Superparamagnetic iron oxide: clinical application as a contrast agent for MR imaging of the liver. Radiology 1988; 168:297–301.
19. Ros PR, Freeny PC, Harms SE, et al. Hepatic MR imaging with ferumoxides: a multicentric clinical trial of safety and efficacy in the detection of focal hepatic lesions. Radiology 1995; 196:481–488.
20. Winter TC, Freeny PC, Nghiem HV, et al. MR imaging with IV superparamagnetic iron oxide: efficacy in the detection of focal hepatic lesions. AJR 1993; 161:1191–1198.
21. Couinaud C. Le foie: études anatomiques et chirurgicales. Paris, France: Masson, 1957.
22. Soyer P. Segmental anatomy of the liver: utility of a nomenclature accepted worldwide. AJR 1993; 161:572–573.
23. Dodd GD III. An American's guide to Couinaud numbering system. AJR 1993; 161: 574–575.
24. Begg CB, McNeil BJ. Assessment of radiologic test: control of bias and other design considerations. Radiology 1988; 167:565–569.
25. Metz CE. ROC methodology in radiologic imaging. Invest Radiol 1986; 21:720–723.
26. Hanley JA, McNeil BJ. The meaning and use of the area under a receiver operating characteristic (ROC) curve. Radiology 1992; 143:29–36.
27. Metz CE. Some practical issues of the experimental design and data analysis in radiological ROC studies. Invest Radiol 1989; 24:234–245.
28. Metz CE. Quantification of failure to demonstrate statistical significance: the usefulness of confidence intervals. Invest Radiol 1993; 28:59–63.
29. Fretz CJ, Stark DD, Metz CE, et al. Detection of hepatic metastases: comparison of contrast-enhanced CT, unenhanced MR imaging, and iron-oxide enhanced MR imaging. AJR 1990; 155:763–770.
30. Vogl TJ, Hammerstingl R, Pegios W, et al. The value of liver specific superparamagnetic contrast medium AMI-25 for the detection and differential diagnosis of primary liver tumors versus metastases. ROFO 1994; 160:319–328.
31. Denys A, Arrivé L, Servois V, et al. Hepatic tumors: detection and characterization at 1-T MR imaging enhanced with AMI-25. Radiology 1994; 193:663–669.
32. Marchal G, Hecke PV, Demaerel P, et al. Detection of liver metastases with superparamagnetic iron oxide in 15 patients: results of MR imaging at 1.5 T. AJR 1989; 152:771–775.
33. Rummeny EJ, Wernecke K, Saini S, et al. Comparison between high-field-strength MR imaging and CT for the screening of hepatic metastases: a receiver operating characteristic analysis. Radiology 1992; 182:879–886.
34. Yamamoto H, Yamashita Y, Yoshimatsu S, et al. Hepatocellular carcinoma in cirrhotic livers: detection with unenhanced and iron oxide-enhanced MR imaging. Radiology 1995; 195:106–112.
35. Fretz CJ, Elizondo G, Weissleder R, Hahn PF, Stark DD, Ferrruci JT Jr. Superparamagnetic iron-oxide enhanced MR imaging: pulse sequence optimization for detection of liver cancer. Radiology 1989; 172:393–397.
36. Hamm B, Reichel M, Vogl TJ, Taupitz M. Superparamagnetic iron particles: clinical results in the MR diagnosis of liver metastases. ROFO 1994; 160:52–58.
37. Edelman RR, Siegel JB, Singer A, Dupuis K, Longmaid HE. Dynamic MR imaging of the liver with Gd-DTPA: initial clinical results. AJR 1989; 153:1213–1219.
38. de Lange EE, Mugler JP III, Bosworth JE, et al. MR imaging of the liver: breath-hold T1-weighted MP-GRE compared with conventional T2-weighted SE imaging: lesion detection, localization, and characterization. Radiology 1994; 190:727–736.